Technical Report
RAL-TR-97-021

An Imaging Neutron Beam Monitor Using Gas Microstrip Technology

J E Bateman N J Rhodes and R Stephenson

May 1997

COUNCIL FOR THE CENTRAL LABORATORY OF THE RESEARCH COUNCILS

Enquiries about copyright, reproduction and requests for additional copies of this report should be addressed to:

The Central Laboratory of the Research Councils
Library and Information Services
Rutherford Appleton Laboratory
Chilton
Didcot
Oxfordshire
OX11 0QX
Tel: 01235 445384 Fax: 01235 446403
E-mail library@rl.ac.uk

ISSN 1358-6254

AN IMAGING NEUTRON BEAM MONITOR USING GAS MICROSTRIP TECHNOLOGY

J E Bateman, N J Rhodes and R Stephenson

Rutherford Appleton Laboratory, Chilton, Didcot, OX11 0QX, U.K.

ABSTRACT

The performance of a new position-sensitive beam monitor for slow neutrons on the ISIS spallation neutron source is reported. Based on gas microstrip technology developed at RAL for particle physics applications, the monitor delivers a sub-millimeter spatial resolution combined with a fast timing response, high data rate capability and a low gamma sensitivity.

1. INTRODUCTION

Each of the 17 neutron scattering instruments at ISIS operates a number of beam line monitors to measure neutron beam intensities at various points in the beam lines. To date these have been scintillation monitors using GS20 glass. These have been very successful but are somewhat sensitive to gamma radiation and offer no information on the distribution of neutron intensity and energy within beam profiles.

There are now a number of areas where position sensitive beamline monitors would be advantageous. Transmission measurements of engineering samples can be analysed to provide structural information about the samples. Resonance radiography requires two dimensional monitor readout. Position sensitive beam line monitors will allow more accurate determination of corrections for sample absorption. They will permit collimation-defining beam line components to be more accurately placed, improving signal to noise ratios. Beam profiles of instruments incorporating neutron guides such as HRPD and IRIS are non-homogeneous with respect to energy. Position sensitive monitor readouts will allow these profiles to be accurately determined.

The lithographic gas microstrip detector (MSGD) was introduced by Anton Oed of the ILL and has been developed by him and his colleagues as a detector of scattered neutrons [1]. At RAL we have concentrated on the application of the MSGD in particle physics, and in particular on the aspects of high counting rates and long lifetimes demanded by application at the LHC at CERN. One outcome of this programme was a prototype beam tracking chamber which was tested successfully in high rate beams [2]. This device has an active area of 82mmx60mm defined by 272 strip sections of 0.3mm width, each section being 60mm high. The lithographic pattern of 10μm wide anodes interleaved with 90μm wide cathodes is produced in a gold process on Schott S8900 semiconducting glass. The active depth of the conversion space is 3mm.

These beam tracking chambers provide a useful means of evaluating the potential of gas microstrip technology in neutron beam imaging. Sufficient readout electronics were available to mount a test at the Pressure and Engineering Applications Beam Line (PEARL) at ISIS.

2. ISIS BEAMS

The PEARL Beam used for our tests is fairly typical of ISIS beams delivering a mean flux of $\approx 10^7 n/cm^2/s$ over an area of $\approx 30 cm^2$. Clearly a detector which subdivides the beam area into small independent counting sections is at an advantage when dealing with potentially large data rates. By the same token a high detection efficiency is not necessary (or desirable) in a beam monitor. With an average detection efficiency of the order of 1%, count rates are expected to approach 100kHz in a 1mm wide strip. Neutron intensity at the sample positions is modulated on a 50Hz cycle in synchronisation with the ISIS pulsed proton beam. Neutron counts from a detector or monitor are time stamped and histogrammed into time bins by the ISIS Data Acquisition Electronics (DAE). The widths of the time bins can be programmed in a variety of ways. The minimum bin width is 0.25μs which determines the time resolution requirement of the counter.

A large amount of gamma contamination is present at short times of flight (short wavelengths) and the intense "gamma flash" as the proton beam hits the target can cause saturation problems to a gamma-sensitive detector.

3. THE DETECTION OF NEUTRONS IN A MSGD

Two problems immediately arise in a gas-filled neutron detector: (i) a converter must be present for the neutrons to give a detectable charged product and (ii) the range of the charged products must be constrained to give the spatial resolution required. In a detector for scattered neutrons these requirements usually combine to enforce the use of gas pressures of several bar. However, in the present case, the combination of a low efficiency and a spatially sensitive detector presents us with the opportunity to realise spatial resolution of 1mm at ambient pressure.

Consider our beam tracking chamber filled with a gas mixture of 50% ^{3}He and 50% CO_2. The active depth (normal to the beam) is 3mm which at a wavelength of 1A gives a calculated detection efficiency of 1.2%. As shown below, this efficiency yields an appropriate counting rate in an ISIS beam. The reaction products of the neutron interaction in ^{3}He are a triton of 200keV and a proton of 570keV. Using the particle range data from ref. [3] shows that the triton has a range of 3.6mm and the proton a range of 13.6mm. The specific energy loss along the particle tracks has an initial value of 32keV/mm for the proton and 54keV/mm for the triton, both peaking at 71keV/mm 1mm before the end of their tracks. In the 3mm active depth of the tracking chamber the proton will in general escape from the conversion region before depositing a significant fraction of its energy. Further, if the MSGD readout is arranged to work in strips of 1mm width, setting a threshold of $\approx$ 100keV in our electronic discriminators ensures that a proton track can virtually never trigger our readout. The spatial resolution of the detector is thus determined by the combined triton and (initial) proton energy total being deposited within a 1mm wide strip. Clearly, there is a trade-off between spatial resolution and detection efficiency: the higher the threshold the lower the detection efficiency and the higher the spatial resolution.

A threshold setting of 100keV should also ensure that the gamma sensitivity of the MSGD is minimised. The density of the counter gas is $\approx$ 1mg/cc which will result in an energy loss of only 0.45keV from a minimum ionising particle crossing the 3mm drift space normally. The worst case of a slow delta ray with a range of 3mm normal to a strip will give an energy deposit of $\approx$ 12keV, well below our trigger threshold. When delta ray tracks are oriented parallel to the plate, in general they pass over many strips, so reducing their ability to trigger the electronics. This insensitivity to fast electrons should be more than adequate to suppress the gamma-induced events in the high Z elements which comprise the MSGD plate.

4. DETECTOR AND READOUT ARRANGEMENT

The particle physics beam chamber has a plate with an anode pitch of 0.3mm. Since a resolution of $\approx$ 1mm is required it is convenient to bus the anode connections in groups of 4 on the plate motherboard. This also reduces the number of electronic channels required. By using 3 standard (16 channel) amplifier cards [2] 48 channels of readout are obtained giving

an active width of 58mm. The active height of the counter (along the strips) is 60mm. The amplifier noise penalty induced by bussing the strips (a fourfold increase in load capacitance) is more than offset by the 100-fold signal increase in the triton signal relative to the usual minimum ionising particle signal. The amplifiers give amplitudes of $\approx$4mV/keV of energy deposit in the detector with a rise time of $\approx$50ns (set by the detector) and a recovery time constant of 100ns.

For the discriminators we used 6 commercial 8-fold NIM units (NE 4684), the outputs of which were used to drive the inputs of 12 ISIS data input modules (MIM).The MIM modules constitute the front end of the ISIS DAE system. The signals from the standard scintillation beam monitor were also recorded via a spare MIM channel.

The counter was filled with a gas mixture of 50%^{3}He and 50%CO_2 by a simple flow method before being sealed. As the counter was not designed for sealed operation (having melinex windows and poor seals) a limited gas lifetime ($\approx$2 days) was observed; however, this was quite long enough for the current tests. The HT biases applied to the counter were: -2.5kV on the drift electrode and -811V on the cathode strips (the anodes being at earth).

In a detector array in which a physical event can simultaneously trigger adjacent channels, the differential linearity is a sensitive function of the gain uniformity of the individual channels. Measurement showed that in the present case the physics amplified the rms gain spread in the electronic channels by a factor of 3.4. A study of the various components of our electronic chain showed the following standard deviations among the 48 channels: amplifier gains - 2.6%, amplifier calibration capacitors - 9.96% and discriminator monitor errors: - 11.9%. (The gain uniformity of the counter is rather better than 2% [2]). Thus calibrating the system using test pulses could be expected to yield a differential linearity of $\approx$35%. This was in fact observed in our first test and dictated that the beam be used to normalise the counter response. Using the relatively flat central section of the beam the discriminator thresholds were adjusted to give the same counting rate (as measured against the scintillator monitor) to within a tolerance of $\approx$2%. This was done in overlapping groups of 10 channels. The threshold was set to an energy equivalent of approximatey 120keV deposited in the detector (as calibrated by the 5.9keV x-rays from ^{55}Fe).

5. RESULTS

The MSGD was installed in PEARL approximately one meter downstream from sample position 3 at 17m from the moderator. The scintillation monitor was situated 4m upstream of the MSGD and the following results recorded.

Figure 1 shows the time spectra recorded by the MSGD and the scintillation monitor. The main difference in the spectra is due to the 4m flight path between the two detectors. The two absorption features in the MSGD spectrum are due to aluminium beam windows in the flight path. The most interesting comparison between the two detectors is the counting rate at short times. Adjusting the curves to take out the effect of the 4m separation and peak normalising the curves at the maxwellian peak allows us to compare the spectra in figure 2. Here we see the scintillation monitor counting a factor of 20 times faster than the MSGD at short times. This is due to the sensitivity of the scintillation monitor to the gamma fluorescence from the

ISIS target. That the signal visible in the MSGD is essentially neutrons is confirmed by the clear sign of nuclear resonances in the signal. In considering the comparison made in figure 2 it must be recalled that the scintillation monitor is 4m nearer the moderator than the MSGD and therefore likely to experiencing a higher gamma contamination in the beam than is present at the MSGD position.

The difference in the gamma responses of the two monitors is shown very clearly by figure 3. This shows the amplifier pulse from the MSGD (upper trace) and the digital pulses from the scintillation monitor (lower trace) on a repetitive digital oscilloscope exposure. On the lower trace we see the gamma flashes producing complete saturation of the scintillation monitor followed by a dead interval of $\approx 1.5\mu s$ during which the system is recovering. On the MSGD trace the gamma flashes can be seen as small baseline blips (nothing can be observed in the digital output) and in the $1.5\mu s$ after the proton bunch very large pulses can be observed as the prompt (MeV) neutrons are detected.

The time resolution of the MSGD counter depends on the drift velocity of electrons in the $^3He/CO_2$ gas mixture. This has not been measured explicitly but figure 3 shows that the pulse fall time of the detector is $\approx 50ns$. This figure is approximately equal to the discriminator time jitter which is thus about an order of magnitude faster than the DAE timing resolution.

The spatial resolution was measured by means of a slit made by separating two 10mm thick sheets of sintered boron carbide apart with 1mm spacers. Because of their size the sheets could not be placed closer than 50mm to the front of the detector. Figure 4 shows the response of the detector system to this collimated beam in the cases of (left) the lowest practical discriminator threshold and (right) approximately twice this threshold value (at which the detector sensitivity is approximately half its former value). Figure 5 shows the response as the detector is moved across the slit using a traversing table. Clearly the spatial response is perfectly linear.

When the central peak of the response is shared between two channels it is possible to fit the observed distribution to the sum of three gaussians with great accuracy. In this case it is observed (figure 6) that 77.1% of the events lie in the narrowest gaussian - σ = 0.55mm, 16.8% in the next widest - σ = 2.13mm and 6% in the widest - σ = 18.34mm.

The trade-off between the spatial resolution and the detection efficiency was explored by varying the counter gain to change the effective energy threshold of the discriminators. Figures 7 and 8 show the standard deviations and the fraction of events in each of the three gaussians as a function of the relative counting rate (normalised to the highest rate). Figure 7 shows that the widths of the narrowest peaks decrease significantly while the widest one does not change as much. The fraction of counts in the two narrow peaks form an approximate zero sum while the fraction in the widest peak remains approximately constant.

When the counter was exposed to the central part of the uncollimated beam a smooth, near-gaussian distribution was observed. A gaussian fit to the observed profile gave a fractional rms error of 2.6%, close to the threshold discriminator errors. Using the residuals as correction factors for independent data sets reduced the rms error to 1%. However, it was clear that the underlying beam distribution had a systematic variation relative to the gaussian

which could be fitted by a small component of polynomial (5th order). Applying this final correction reduced the fixed pattern errors in the detector to 0.6% (limited now by counting statistics in the calibration data).

Figure 9 shows a scan across the entire beam profile requiring two shifts of the detector. The central portion of the beam clearly approximates to a gaussian with $\sigma = 28.18$mm. However, there are systematic variations in the centre and the wings are clipped.

Figure 10 shows the beam profiles in three distinct time of flight bands (i.e. wavelength bands). As can be seen there is no detectable change in the PEARL beam profile as a function of neutron wavelength. In a guided beam one would expect the situation to be more complex. The changes of the vertical scale with the time band are a result of the greater sensitivity of the scintillator monitor to gammas, particularly at the lower wavelengths. In the lower data set the overlaps of the three detector positions have been included to show that the detector normalisation is independent of the beam position at which it was calculated.

6. DISCUSSION

The performance of the MSGD beam monitor may be discussed under the following headings:

Spatial Resolution

Figures 4,6 and 7 show that over the working range available the spatial resolution has a principal component which is comfortably sub millimeter (standard deviation). Since the collimator slit is 1mm and the detector element is 1.2mm wide it is impossible to quantify the resolution at 50% acceptance better than this. The approximately zero-sum behaviour of the two narrowest gaussians (figure 8) suggests that, as the threshold varies, the triton and proton track orientations are differentially selected. Large energy deposits correspond to tracks which lie parallel to the longer dimensions of the strip active volume and hence yield good spatial resolution in the direction of measurement.

The very wide, low-level gaussian (#3) is clearly centred on the slit but is little affected by the discriminator level which suggests that it is an artefact of the experimental set-up rather than a property of the detector itself. It is narrower than the beam and tracks with the slit. Therefore it is probably due to scattering off the deep (10mm) jaws of the slit which was forced to be 50mm away from the detector by the geometrical constraints of the set-up. A more sophisticated double slit collimator would eliminate this distribution.

A further possible scattering contribution arises from the melinex window which is estimated to scatter about 1% of the incident beam. The window is located 5mm in front of the active detector volume and its scatter distribution will overlap with the second gaussian distribution ($\sigma \approx 2$mm).

Time Resolution and Rate Capability

As noted above, the time resolution of the detector is of the order of the fall time of the

analogue pulse seen on the top trace of figure 3, i.e. about 50ns. In the present tests the maximum average rate observed in a single strip was about 10kHz with a peak rate of perhaps three times that rate. Distributed as they are over 60mm of anode length the count rate density is at least two orders of magnitude below the limits already demonstrated for this detector [2]. In respect of time-domain characteristics the MSGD will meet any forseeable requirement on ISIS.

Detection Efficiency

It is estimated that the MSGD beam monitor stops 1.2% of neutrons incident at 1A. There is no very precise way to check the sensitivity experimentally. However, within the constraints of our knowledge of the beam geometry the estimated sensitivity of the scintillation monitor (10^{-4} at 1A) can be used to give an approximation. This calculation shows that the detection efficiency of the counter at maximum sensitivity is 0.14%. Because the MSGD is four meters downstream of the monitor and the beam divergence is not known, the relative fraction of the beam intercepted by the scintillation monitor and the MSGD at their respective locations is not well known. From figure 9 it is estimated that the MSGD intercepts about 50% of the beam at its location so the figure of 0.14% is probably a lower limit. The low detection efficiency relative to the neutron stopping efficiency ($\approx 10\%$) is due to the severe selection imposed on the pulse height spectrum in the detector by the high (120keV) discriminator threshold.

Gamma Sensitivity

No explicit measurements of the gamma sensitivity of the MSGD were made. However, the evidence of figures 2 and 3 is that the gamma sensitivity is dramatically lower than that of the scintillation monitor. In particular, figure 2 shows that in the region of the nuclear resonances, the absorption features are deep and sharp, indicating that there is little, if any, gamma contamination. A further confirmation of the gamma insensitivity is given by the response of the detector to the slit beam (figure 6 for example). Approximately 98% of the beam stops in the boron carbide collimator and 93% of the absorbed neutrons generate a 480keV gamma ray of which perhaps 20% will pass through the MSGD. Any significant detection of these gamma rays would show an image of the beam and nothing of the sort is observed. This insensitivity to gamma rays is not surprising since it is all but impossible for a delta ray to deposit 100keV in the volume defined by a counter strip.

7. FUTURE DEVELOPMENTS

Since the MSGD used for these tests has an intrinsic strip width of 0.3mm, we plan to explore the lower limit of spatial resolution achievable in this device. Using CF_4 in place of CO_2 halves the triton and proton ranges and may well enable spatial resolution in the sub-half-millimeter range to be achieved.

In order to achieve 2-D imaging of neutron beams we plan to install a second dimension readout wire plane in our MSGD and expect to achieve comparable spatial resolution in the direction orthogonal to the MSGD strips.

Any significant increase in the neutron detection efficiency of the MSGD monitor will require pressurisation. Studies are in hand of the engineering problems and (by means of a montecarlo model) of the optimal trade-off between spatial resolution and detection efficiency.

REFERENCES

1. A Oed, Nucl Instr & Meth A263 (1988) 351-359
A Oed et.al., A large, high counting rate, one-dimensional, position sensitive n-detector: the D20 banana, submitted to Physica B: Physics of Condensed Matter.

2. J E Bateman, J F Connolly, R Stephenson, M Edwards and J C Thompson, Nucl. Instr. and Meth. A348 (1994) 372

3. J F Janni, (1982) Atomic Data and Nuclear Data Tables, 27, Nos 2-5

FIGURE CAPTIONS

Figure 1 Typical time of flight spectra obtained during the test of the MSGD beam monitor on the PEARL Beam at ISIS. The scintillation monitor spectrum arrives earlier because it is approximately 4m nearer the moderator.

Figure 2 A comparison of the time of flight spectra of figure 1 at short times. The spectra have been adjusted for the flight path difference.

Figure 3 A repetitive storage oscilloscope trace of the pulse streams from the MSGD (top) and the scintillation monitor (bottom). (The top trace shows amplifier pulses and the lower disciminator pulses.)

Figure 4 The spatial response of the MSGD to a slit beam (1mm wide) with the lowest threshold used (left, 100% acceptance) and the highest (right, 50% acceptance).

Figure 5 The spatial response of the MSGD as it is scanned across the slit beam in steps.

Figure 6 A "three gaussian" fit to the slit beam image at 50% acceptance. The table shows the number of counts and the σ for each gaussian.

Figure 7 The standard deviations of the three gaussians as the acceptance (energy threshold) is varied.

Figure 8 The fraction of the counts in each gaussian as the acceptance (energy threshold) is varied.

Figure 9 A composite 1-D image of the whole neutron beam, obtained in three separate exposures with the MSGD moved between exposures. A gaussian fit to the central portion is shown. In the orthogonal direction the MSGD intercepts about 50% of the beam. The counts have been normalised to counts from the scintillation monitor recorded at the time.

Figure 10 1-D images of the beam in three neutron wavelength bands. The lower normalisation of the short wavelength band is due to the gamma sensitivity of the scintillation monitor.

FIGURE 1

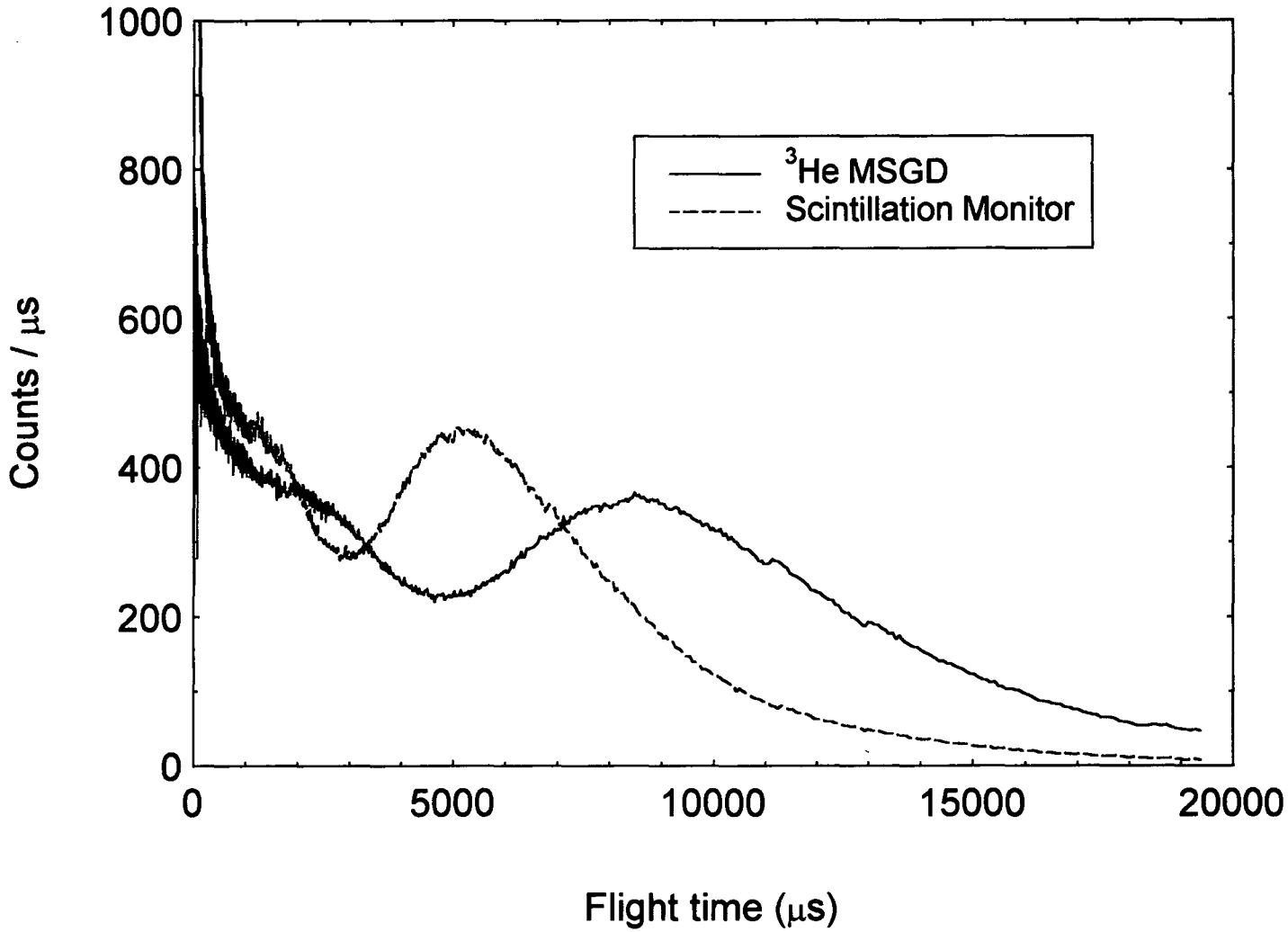
1000
800
600
400
200
0
Counts / μs
0
5000
10000
15000
20000
Flight time (μs)
^{3}He MSGD
Scintillation Monitor

FIGURE 2

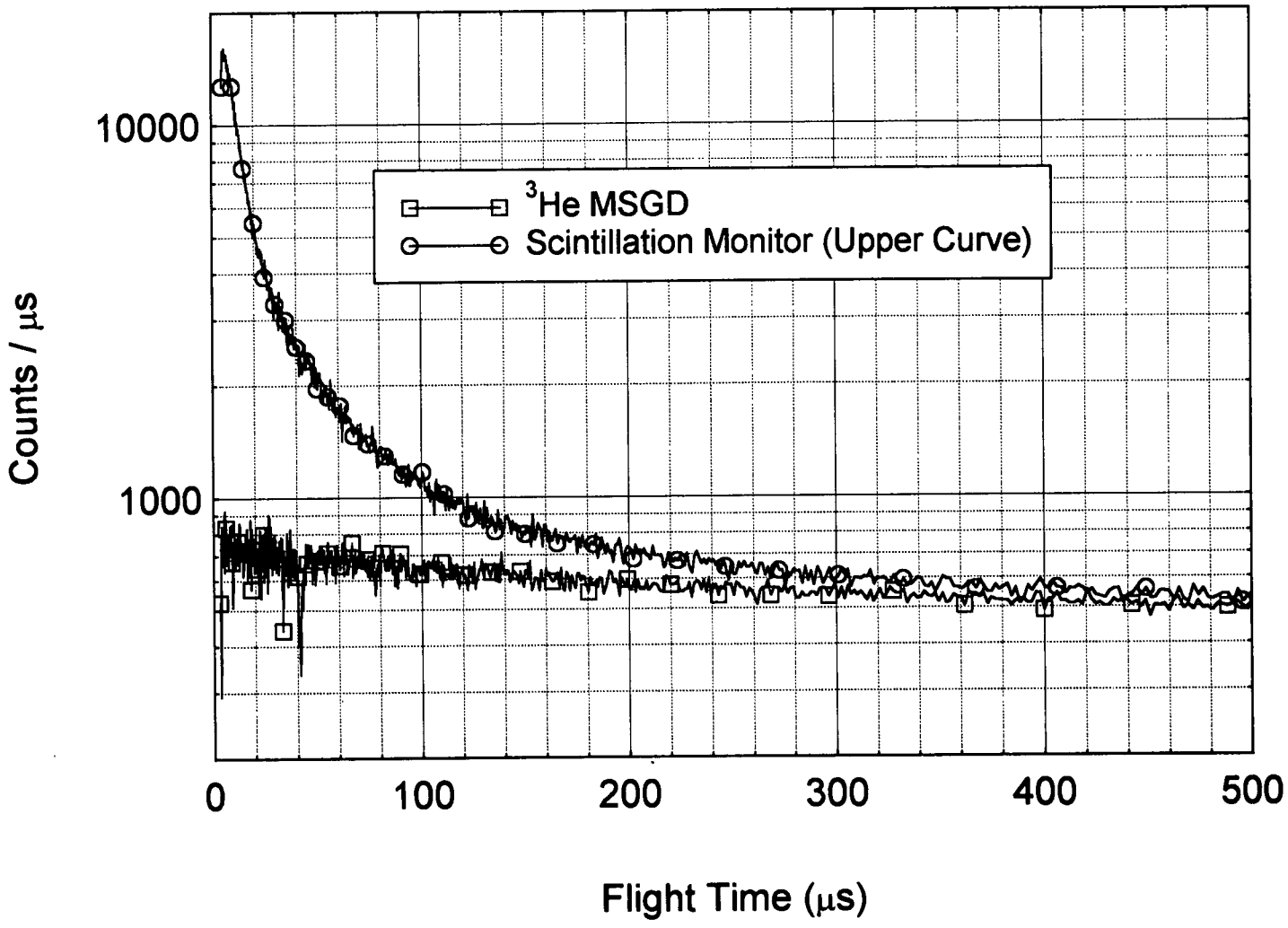
10000
1000
Counts / μs
^{3}He MSGD
Scintillation Monitor (Upper Curve)
0
100
200
300
400
500
Flight Time (μs)

FIGURE 3

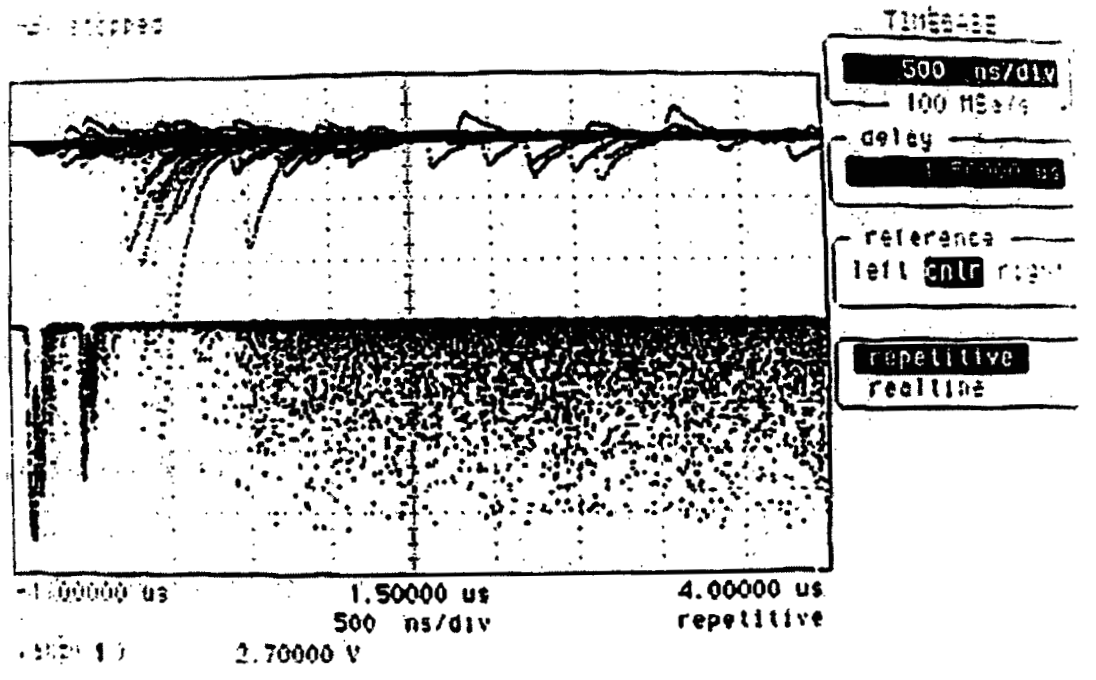
Timebase
500 ns/div
delay
reference
left
repetitive
realtime
1.50000 us
500 ns/div
4.00000 us
repetitive
2.70000 V

FIGURE 4

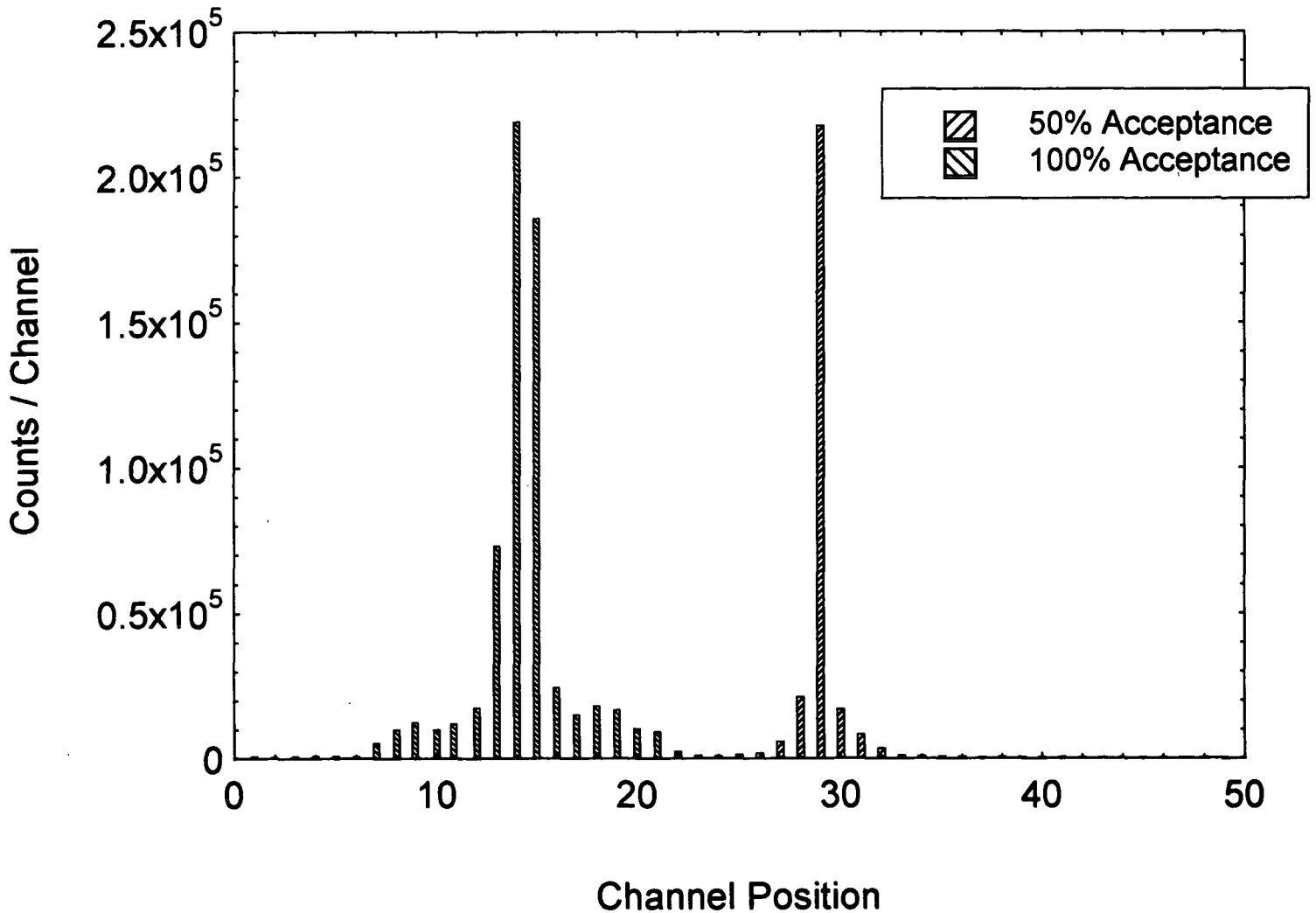
2.5x10^5
2.0x10^5
1.5x10^5
1.0x10^5
0.5x10^5
0
Counts / Channel
0
10
20
30
40
50
Channel Position
50% Acceptance
100% Acceptance

FIGURE 5

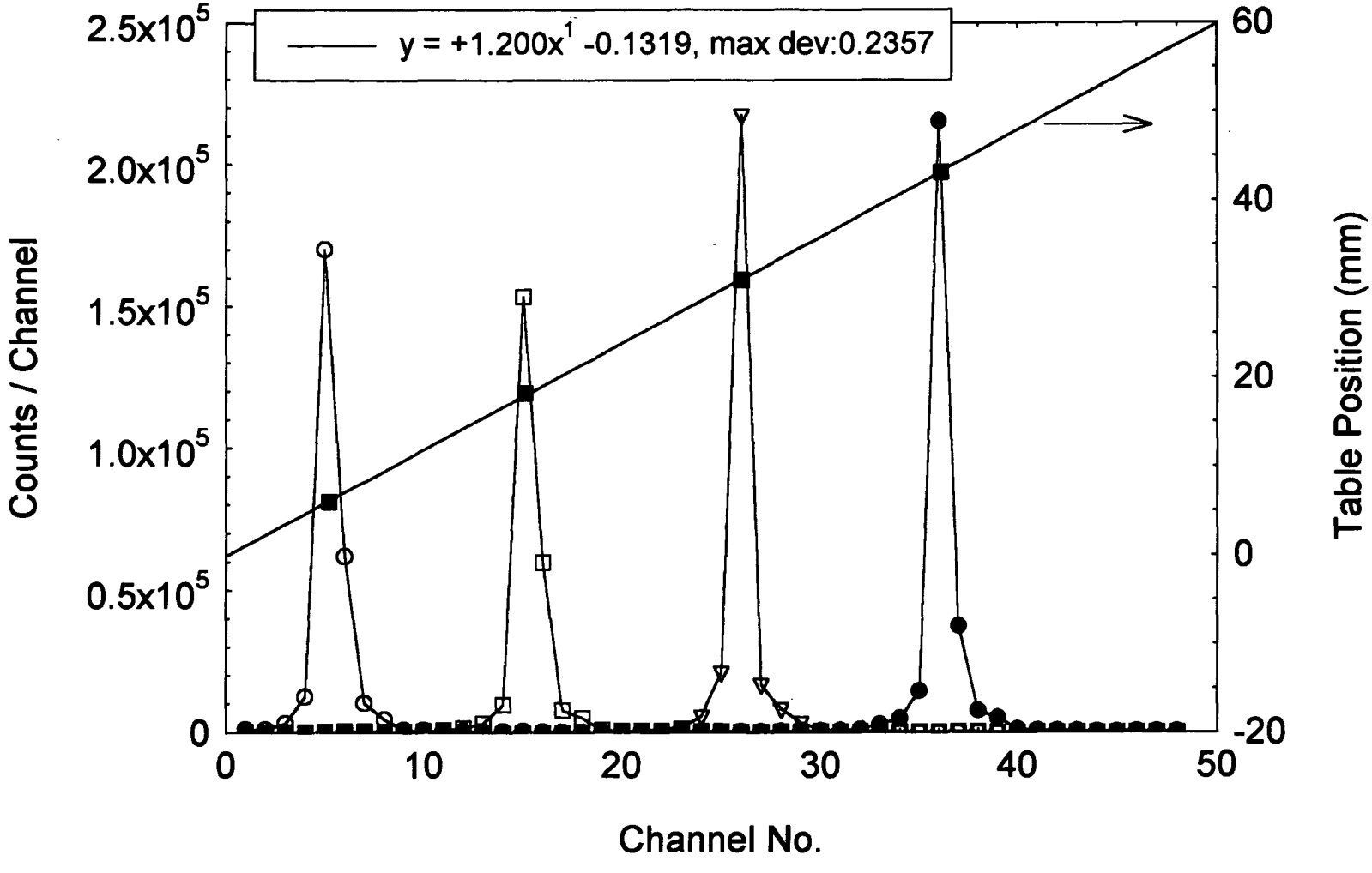
y = +1.200x^1 -0.1319, max dev:0.2357
2.5x10^5
2.0x10^5
1.5x10^5
1.0x10^5
0.5x10^5
0
Counts / Channel
0
10
20
30
40
50
Channel No.
60
40
20
0
-20
Table Position (mm)

FIGURE 6

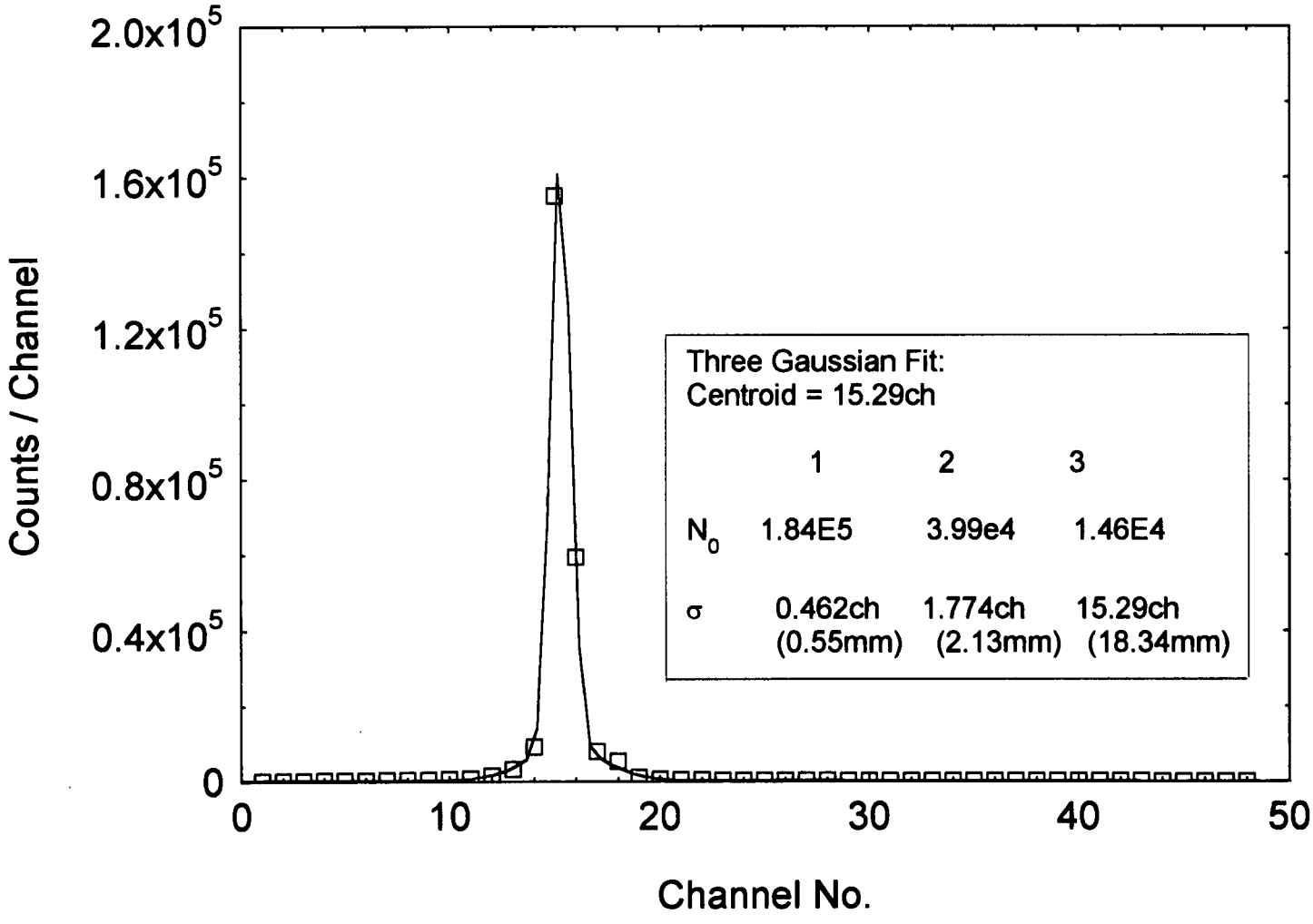
2.0x10^5
1.6x10^5
1.2x10^5
0.8x10^5
0.4x10^5
0
Counts / Channel
0
10
20
30
40
50
Channel No.
Three Gaussian Fit:
Centroid = 15.29ch
1
2
3
N0 1.84E5 3.99e4 1.46E4
σ 0.462ch (0.55mm) 1.774ch (2.13mm) 15.29ch (18.34mm)

FIGURE 7

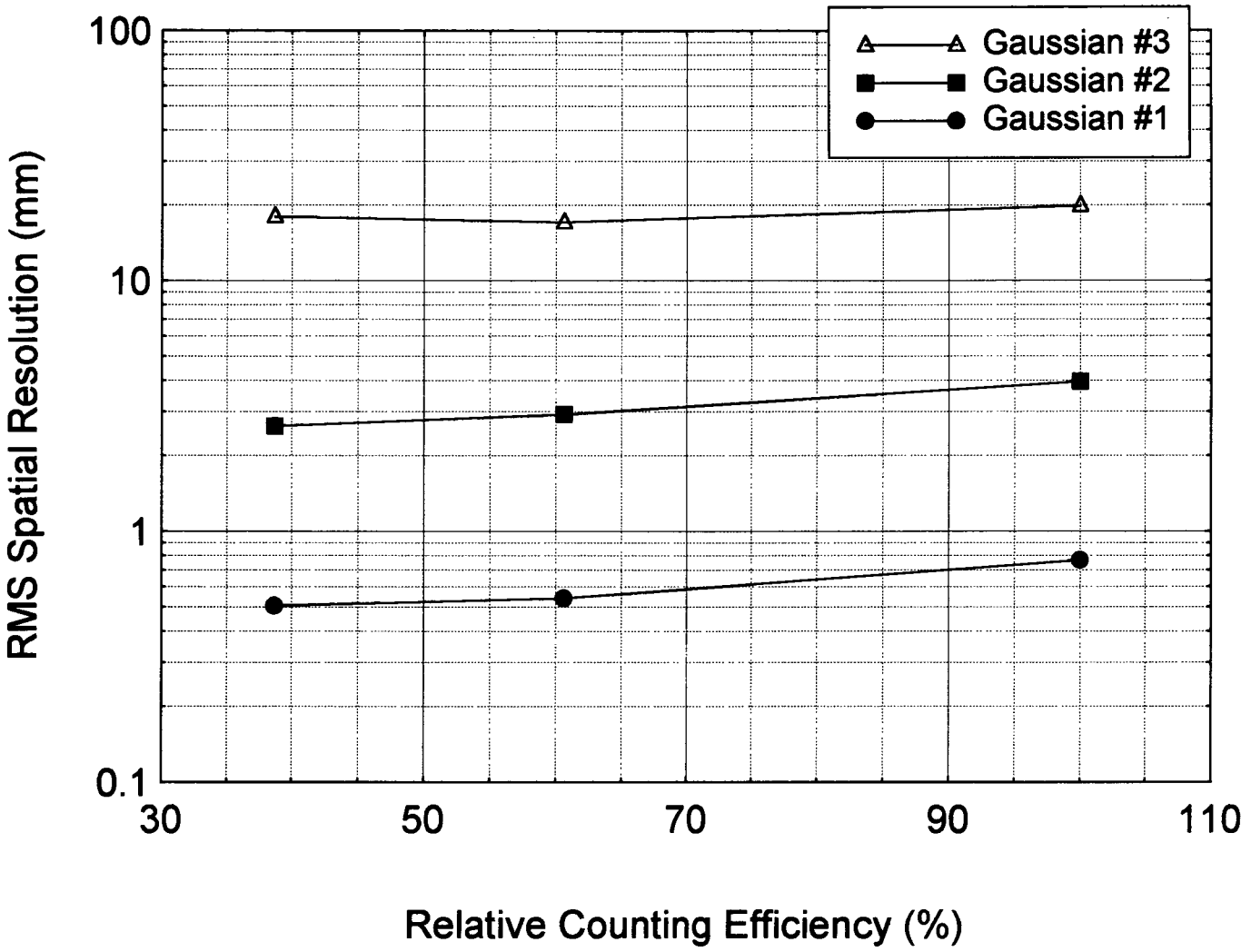
100
10
1
0.1
30
50
70
90
110
RMS Spatial Resolution (mm)
Relative Counting Efficiency (%)
Gaussian #3
Gaussian #2
Gaussian #1

FIGURE 8

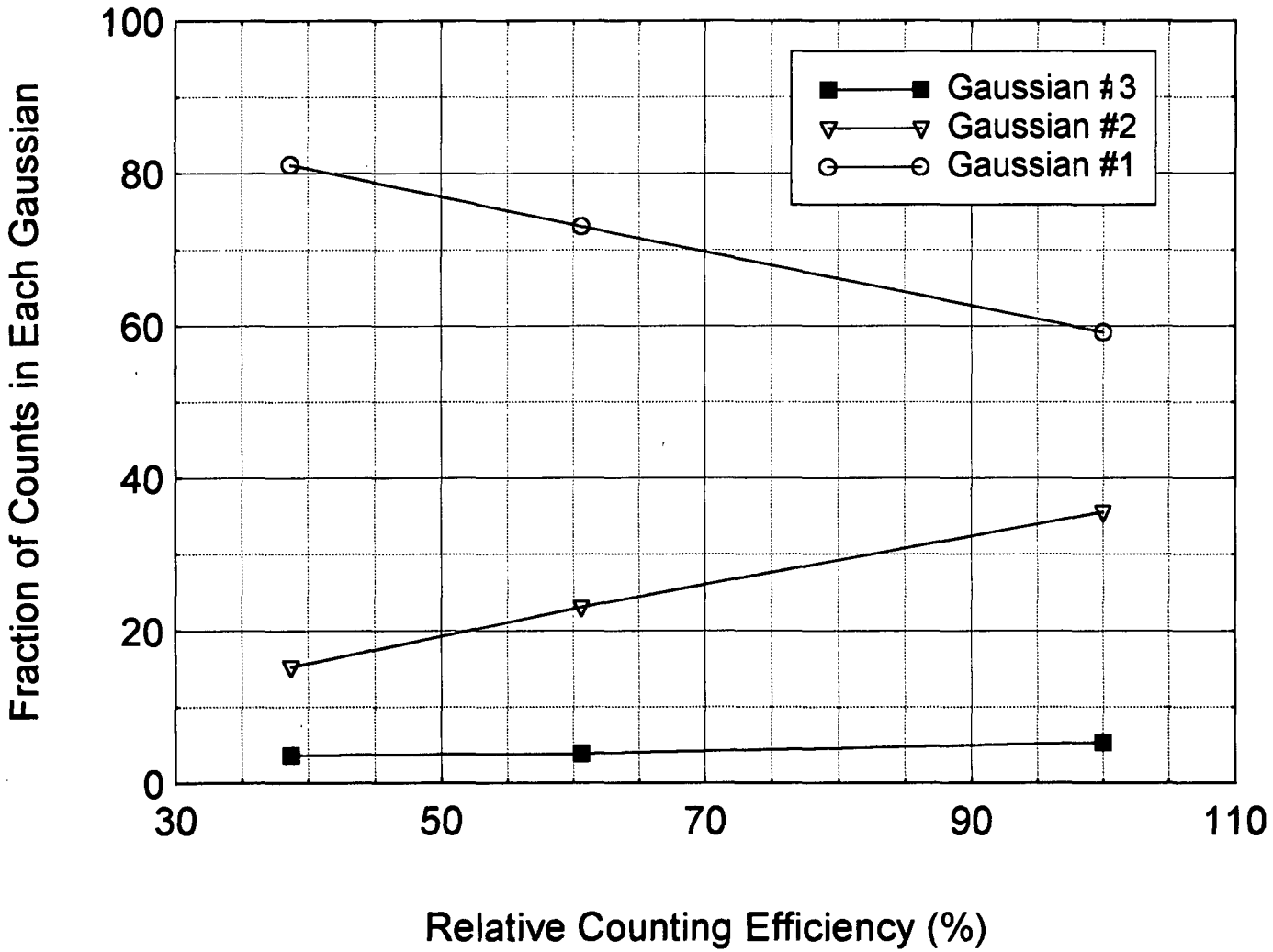
100
80
60
40
20
0
30
50
70
90
110
Fraction of Counts in Each Gaussian
Relative Counting Efficiency (%)
Gaussian #3
Gaussian #2
Gaussian #1

FIGURE 9

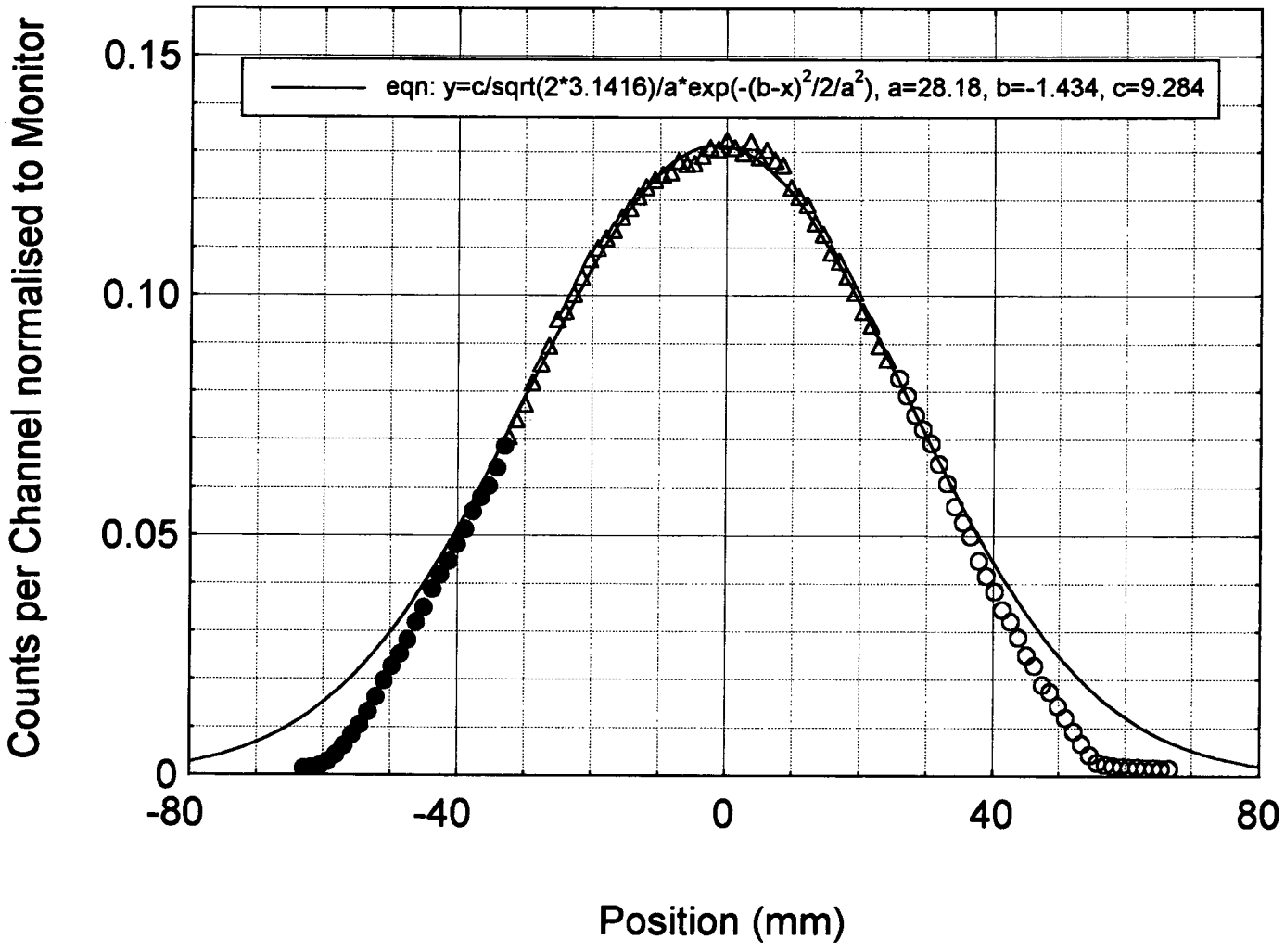
eqn: y=c/sqrt(2*3.1416)/a*exp(-(b-x)^2/2/a^2), a=28.18, b=-1.434, c=9.284
Counts per Channel normalised to Monitor
0.15
0.10
0.05
0
-80
-40
0
40
80
Position (mm)

FIGURE 10

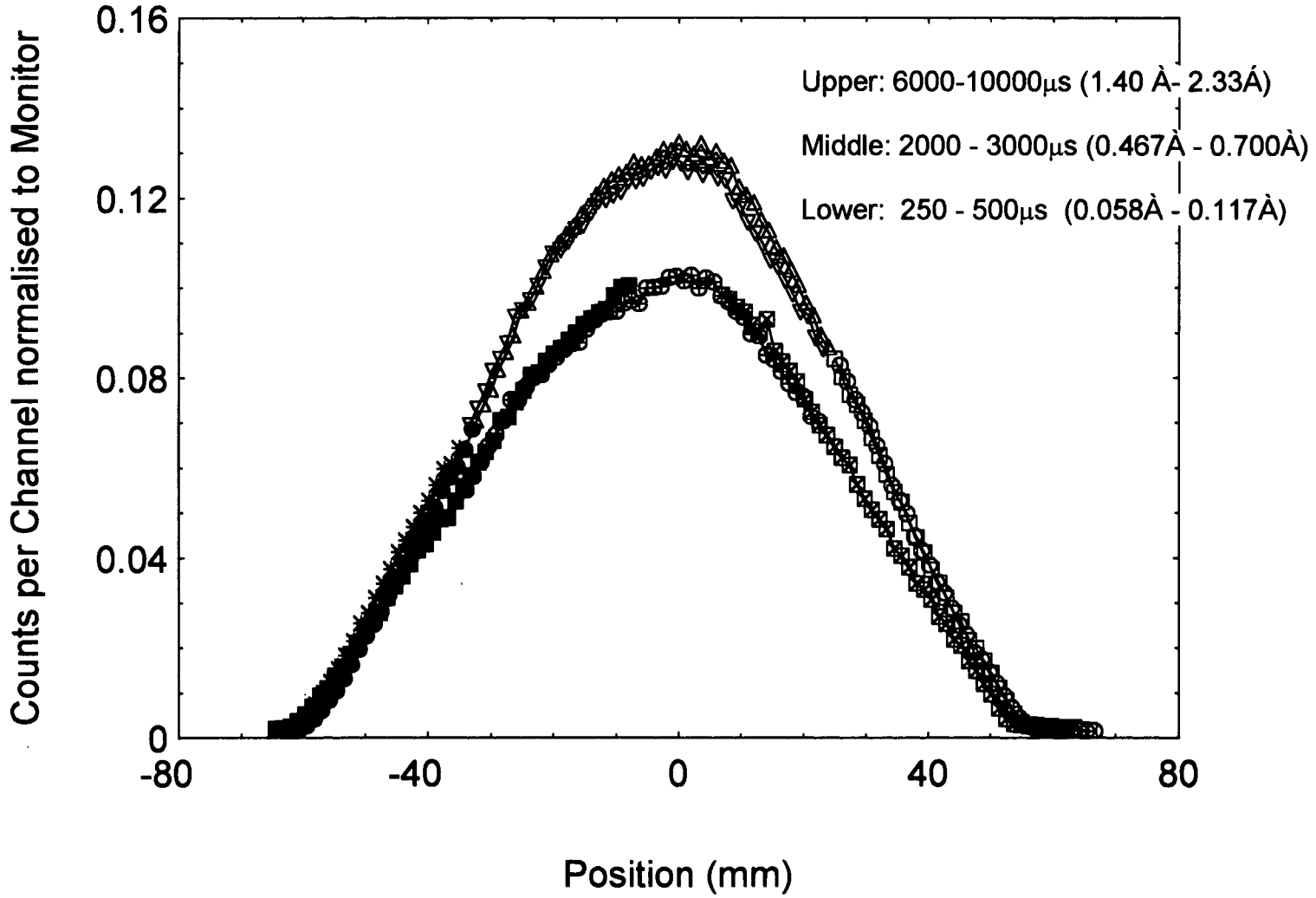
Counts per Channel normalised to Monitor
0.16
0.12
0.08
0.04
0
-80
-40
0
40
80
Position (mm)
Upper: 6000-10000μs (1.40 À- 2.33Á)
Middle: 2000 - 3000μs (0.467À - 0.700À)
Lower: 250 - 500μs (0.058À - 0.117À)